Polar Heterostructure for Multifunction Devices: Theoretical Studies

Yuh-Renn Wu, *Member, IEEE,*, and Jasprit Singh

***Abstract*—In this paper, we examine the potential of devices based on heterostructures made from highly polar materials and semiconductors. Our calculations show that such functional devices have superior sensor properties and transistor properties. The basis device examined is based on the use of a thin oxide with high piezoelectric coefficients or pyroelectric coefficients under the gate region. Channel charge and current are controlled by gate voltage, temperature, or stress. We examine the performance of three classes of heterostructures that form the basis of important semiconductor technologies: 1) Si–SiO_2–$BaTiO_3$ heterostructure junctions that would be an important breakthrough for silicon sensor technology; 2) GaN–AlN–$BaTiO_3$ heterostructure junctions that would be important especially in high temperature sensor application; and 3) GaAs–AlGaAs–$BaTiO_3$ heterostructure field effect transistors. The calculations show that with a very thin polar material layer we can have a highly sensitive sensor and transistor. For optimum performance, the polar material (piezoelectric or pyroelectric) layer thickness should be ~ 30 Å.**

***Index Terms*—Device simulations, GaAs, GaN, piezoelectric, pyroelectric, sensor, silicon, stress sensor, thermal sensor.**

I. Introduction

IF WE examine high-performance electronic and optoelectronic devices, we find that they are made from semiconductors (such as Si, GaAs, InGaAs, etc.). On the other hand, devices that fall in the general category of sensors are made from insulators (a variety of oxides). The dominance of semiconductors in electronic and optoelectronic devices can be traced to two properties (see Fig. 1): 1) A small change in the Fermi level position can alter the density of "free" carriers and conductivities by orders of magnitude; 2) Charge injection can alter the conductivities and optical properties by orders of magnitude. As a result, semiconductor-based devices, such as transistors, diodes, light emitters and detectors, have remarkable performance. Semiconductors also have been applied in many sensor areas, such as silicon strain sensor [1], GaAs FET strain sensor [2], [3], and P-N diode temperature sensors [4]. However, the response to perturbations, such as stress, temperature fluctuation, magnetic field changes, chemical gas, etc., are relatively poor.

Smart materials (traditionally falling in the insulator category) such as $BaTiO_3$, PLZT, KDP, $LiNbO_3$, etc. have excellent piezoelectric, pyroelectric, ferroelectric, and electrooptic properties [5]–[9], which make them attractive for many applications. Sensor devices based on these materials rely upon the fact that a small perturbation (stress, temperature, charge, etc.) produces a large change in the polarization of the material. This polarization change can then be detected as current or voltage signal using semiconductor based devices. Ideally one would like to create heterostructures which have the properties of semiconductors and also the superior polar properties of certain oxides. Such heterostructures will create new choices of devices with applications not only in traditional electronics and optoelectronics but for night vision, stress sensing, chemical sensing, etc.

There are several key reasons for being optimistic about semiconductor-polar material heterostructures: 1) Heterostructures between quite different semiconductors have been shown to have unique properties. These structures are routinely used for high performance devices; 2) Epitaxial technologies such as MBE are being applied to high quality polar oxides and have been shown to offer monolayer control. While such layers have not been exploited for device applications, the high degree of crystallinity of these films shows promise of excellent intrinsic properties (piezoelectric, pyroelectric, magnetic, etc.) [10]–[14]; and 3) Theoretical technologies developed for traditional semiconductor heterostructures (concepts of band lineup, effective mass, $k \cdot p$ theory, etc.) have been modified and applied to polar heterostructures based on nitrides (AlN, GaN, InN, and their alloys) [15]–[17]. Such models have been validated by experiments and have been used for device designs. This suggests that (with modifications) relatively simple quantum mechanisms can be applied to design polar heterostructures. Of course these models will always have to be tested against experiments.

There are many potential ways of incorporating smart materials into semiconductor structures. One can imagine the gate oxide of a field-effect transistor (FET) to be replaced by a smart oxide leading to a "FET-sensor." It is also possible to combine smart oxides (such as $LiNbO_3$) into the Braggs reflector of a DFB laser to produce lasers whose frequency is sensitive to stress or temperature variations, etc.

Regardless of the conceptual nature of the design chosen, one must keep the following concern in the forefront. The oxides will have a high level of defects and therefore in the device design, the free charge in the device should be spatially separated from the polar region and should reside in the semiconductor part. In the Si–SiO_2 technology the two-dimensional electron charge (2DEG) is in the semiconductor although it does suffer from interface roughness scattering. Nevertheless Si–SiO_2 based devices work quite well because the penetration of the carrier wave function into the SiO_2 region is very small.

Manuscript received March 29, 2004; revised October 11, 2004. This work was supported by the U.S. Office of Naval Research under Grants F001681, F004815, and F010682. The review of this paper was arranged by Editor K. Najafi.

The authors are with the Department of Electrical Engineering and Computer Science, University of Michigan, Ann Arbor, MI USA

Digital Object Identifier 10.1109/TED.2004.842546

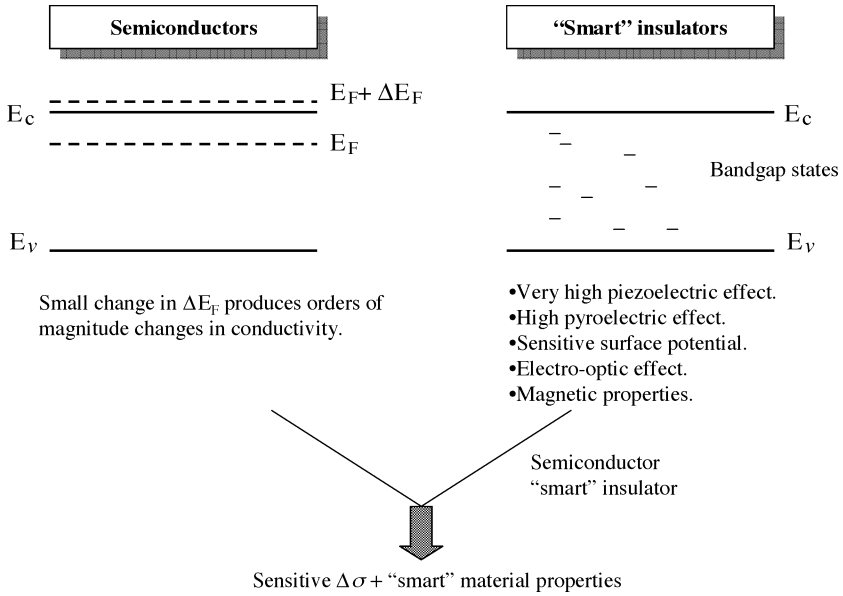

Fig. 1. Semiconductors have the remarkable properties of conductivity and $e - h$ injection control. Smart materials based on various oxides have remarkable polarization, magnetic, and electrooptic properties. The heterostructures between the two classes would lead to novel devices.

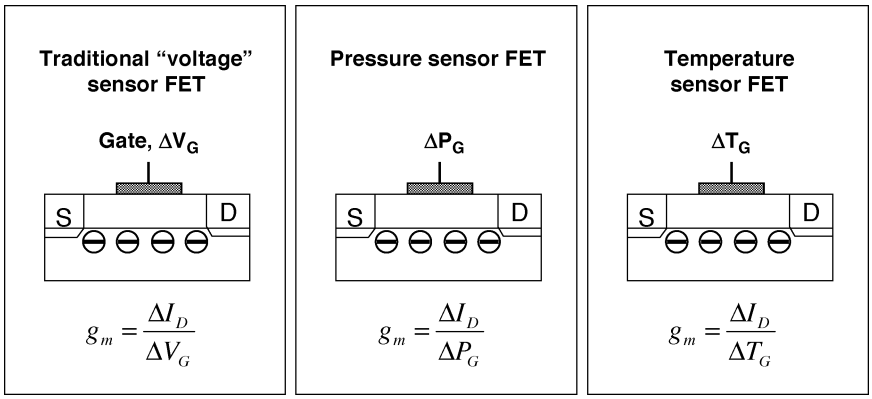

Fig. 2. Schematic of smart sensors based on oxide–semiconductor heterostructures.

In the following sections, we will explore the polarization of a FET where the gate oxide (or large bandgap material) incorporates a material with very high polar (or other) response. The structure will be examined as a FET and as a stress or a thermal sensor. In Fig. 2, we show a generic description of these devices. The first structure represents a traditional FET where a gate voltage V_G controls the channel current I_D. A popular measure of the device performance is the transconductance

$$g_m = \frac{dI_D}{dV_G}. \tag{1}$$

In Fig. 2, we also show the kinds of devices that could arise if thin layers of smart gate oxides can be deposited on top of the semiconductor structure. As noted above, it is important that the region where the free carriers reside is separated from the oxide.

In the smart-FET devices shown in Fig. 2, we consider devices in which the two-dimensional (2-D) channel charge is modulated by stress and temperature change. An appropriate measure of the device performance is a new "transconductance" describing how the perturbation control the channel current

$$\text{"}g_m\text{"} = \frac{dI_D}{dP} \tag{2}$$

where dP is the appropriate perturbation.

In this paper, we will develop a general formalism based on a self consistent charge control model which includes these polarization effects and the quantum solution of the free carrier states to examine a stress sensor-FET. We will examine some typical materials with high piezoelectric coefficients placed above a 2-D electron channel in several semiconductor systems (Si, GaAs, and GaN). Our results will focus on arriving the following questions: 1) What kind of layer thickness is needed to allow a polar gate oxide to influence and control channel charge? and 2) What kind of sensitivity is possible in such a functional device? We will show from a calculation that for these stress-sensor-FETs to operate, the thickness of the polar oxide has to be ~ 30 Å. We will also show results for temperature-sensor-FETs exploiting pyroelectric properties.

As noted above several group have used techniques like MBE to grow high-quality polar oxide structures. These structures are free from pinholes, cracks and dislocations. There are, however, few experimental studies on the polar properties of a very thin film (~20–50 Å). We have used values for piezoelectric and pyroelectric constant from literature which are usually measured for thicker films. It is not clear that if the polar values in thinner films will increase or decrease. Future experiments will allow us to make a model more accurate. The purpose of this paper is to provide a guidance and motivation for experiments.

II. Formalism

Charge control models in semiconductor heterostructures are now covered in most advanced device textbooks. Approaches to self-consistent solutions to the Poisson equation and Schrödinger equations are well known. In the case of polar heterostructures also, such techniques have been developed and compared with experiments for the nitride heterostructure devices. In polar heterostructures, the key modification in charge control models is due to the presence of "fixed" polar charge at various interface arising from the difference in polarization of adjacent layers. We have developed a general formalism to apply to polar heterostructures and have applied it to nitride heterostructures [18]–[20], Detailed comparison with experiments have shown the validity of such an approach.

In discussing polar heterostructures, it is important to identify the various charges present. These are 1) fixed interface charges as noted above. This charge is on the lattice and is not mobile; 2) charges due to dopants; 3) free charge (i.e., electrons or holes) that is mobile. We are particularly interested in 2DEG that can be induced in heterostructure devices.

Before discussing our formalism, we discuss the basic structure of devices considered. The general structure is shown in Fig. 3. For an Si-based device, an oxide SiO_2 with a large bandgap is grown on top of an Si semiconductor as an insulator to stop the leakage current from the gate. In nitrides or arsenides cases, AlN, and AlGaAs are grown on top of GaN and GaAs, respectively. Then a polar oxide, $BaTiO_3$, is grown on top of the insulator. The reason behind the use of a thin SiO_2 (or AlN and AlGaAs in Arsenide and nitride cases) is that their defect properties are well studied and controlled. Therefore, transport properties at the insulator–semiconductor are already optimized in current technologies. In Fig. 3(a), we show the key energy levels associated with the metal, the polar oxide, the insulator oxide, and the semiconductor. When the capacitor is formed, as shown in Fig. 3(b), the Fermi-level is aligned so that there is no gradient. The gate bias is set to 0 in the whole simulation so that we assume no external applied electric bias. At the metal–polar material interface, the fixed negative polarization charge is balanced by the metal contact. At the polar material–insulator interface, there exits a fixed positive polarization, which will cause band bending as shown in Fig. 3(b). The degree of band bending will affect the amount of 2DEG formed at the insulator–semiconductor or polar oxide–insulator interface. To examine the device, we need to develop the following: 1) A model for how the polar charge is influenced by the stress and temperature; 2) A model for band line up between the polar oxide, insulator, and semiconductor structures; 3) A model to account for fixed polar charge; and 4) A quantum model for the 2DEG and its distribution. Before considering the formalism for charge control, we will discuss how stress and temperature influence polar charge.

A. Stress Sensor

We first consider the stress sensor and develop a model that describes how the polar charge and 2DEG vary with stress. The formalism developed is generic and can be applied to other "smart" oxides as well. The basic structure examined by us is shown schematically in Fig. 4(a). As shown, a "smart oxide" (in our simulation, this is $BaTiO_3$) is placed between the gate and 2-D channel of a FET. We note that since at present oxides such as $BaTiO_3$ are likely to have high defect density and very poor mobility, we design the smart FET so that the free carrier density is essentially at the high quality Si–SiO_2 interface. The metal–piezoelectric–insulator–semiconductor FET (MPISFET) sensor is assumed to be grown on silicon cantilever as shown in Fig. 4(b).

When a force $\mathbf{F}$ is applied on the side of the cantilever, the deflection dz in the z direction is given by

$$dz = \frac{L^3}{3EI}\mathbf{F} \tag{3}$$

where E is Young's modulus of the cantilever, I is the momentum of inertia, and L is the length of the cantilever. The momentum of inertia, I, of a rectangular cantilever is $hd^3/12$, where h is the cantilever width and d is the cantilever height. The size of L, h, and d are set to be 200, 200, and 10 μm, respectively. The gate length of sensor-FET is 1 μm in this case. When the cantilever is under force, the stress is given by

$$\sigma_x(x,z) = -\frac{xz}{I}\mathbf{F} \tag{4}$$

$$\sigma_y = \sigma_z = 0 \tag{5}$$

$$\sigma_{xz}(z) = -\frac{1}{2I}\left(\frac{d^2}{4} - z^2\right)\mathbf{F} \tag{6}$$

where σ_x, σ_y and σ_z are the stress in the x, y, and z direction, respectively. The σ_{xz} is the shear stress in $x-y$ direction. When the sensor is grown on top of the cantilever, $z = -d/2$, and σ_{xz} would be 0 for $z = -d/2$. Therefore, we do not need to consider the shear force in this case. From the (3) and (4), the strain ϵ_x can be derived as shown below

$$\epsilon_x\left(x, -\frac{d}{2}\right) = -\frac{xz}{IE}\mathbf{F} \tag{7}$$

$$= \frac{3x\left(\frac{d}{2}\right)}{L^3}dz \tag{8}$$

where $z = -d/2$ since the MPISFET is grown on top of the cantilever. We can also derive that the strain ϵ_y is equal to $-\tau\epsilon_x$, where τ is the Poisson ratio. The detailed formalism can be found in [9]. Here, we have assumed that MPISFETs are much thinner than the height of the cantilever, and therefore the strain, ϵ_x and ϵ_y, on top of the cantilever is equal to the strain on the piezoelectric material. The piezoelectric material, $BaTiO_3$, has

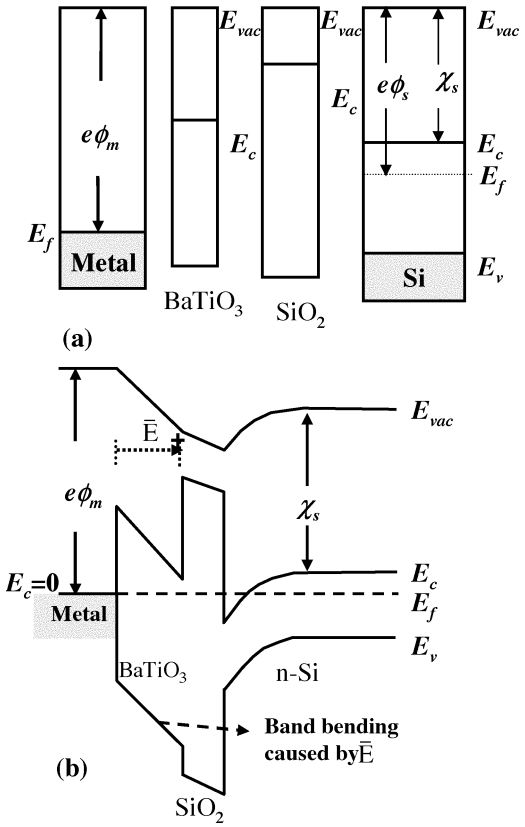

Fig. 3. (a) Band profiles of the isolated metal, the polar oxide, the oxide, and the semiconductor. ϕ_m is metal work function, χ_s is the electron affinity, $E_{\rm vac}$ is the vaccuum energy level, E_c is the conduction energy band, E_v is valence band, and E_f is the Fermi-level. (b) Band profile of the heterostructure junctions.

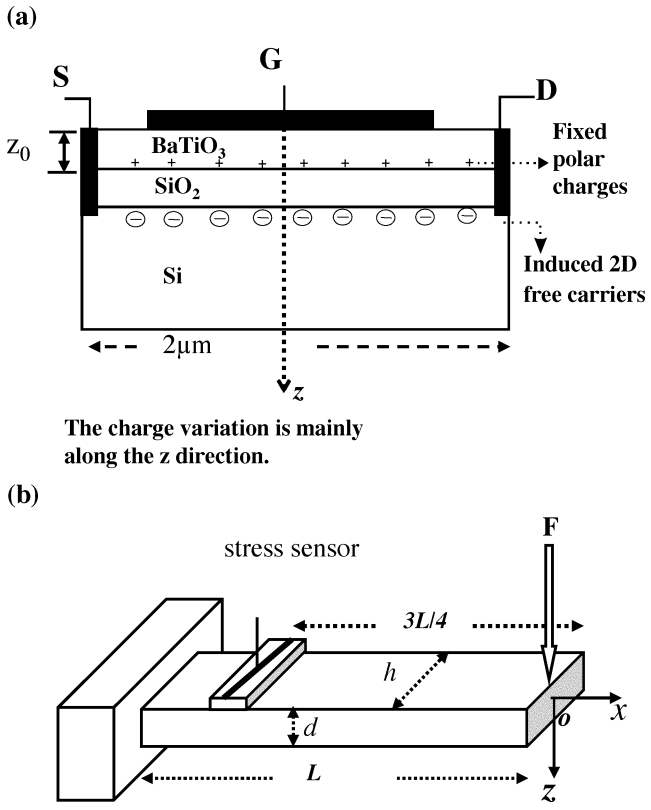

Fig. 4. (a) Schematic of the MPISFETs structure. The gate length is 1 μm. (b) MPISFETs is assumed to be grown on top of the cantilever. L is the total length of the cantilever which is set to be 200 μm. d is the height of the cantilever, which is set to be 10 μm. O is the origin of the Cartesian coordinate. The sensor FET is at $x = 3/4L$.

a tetragonal crystal structure [21]. The elastic constant can be expressed by

$$\sigma_i = \sum_j C_{ij}\epsilon_j \tag{9}$$

where C_{ij} is the elastic constant. For tetragonal structures, with the symmetric reduction the C_{ij} can be simplified to

$$C = \begin{bmatrix} C_{11} & C_{12} & C_{13} & 0 & 0 & 0 \\ C_{12} & C_{11} & C_{13} & 0 & 0 & 0 \\ C_{13} & C_{13} & C_{33} & 0 & 0 & 0 \\ 0 & 0 & 0 & C_{44} & 0 & 0 \\ 0 & 0 & 0 & 0 & C_{44} & 0 \\ 0 & 0 & 0 & 0 & 0 & C_{66} \end{bmatrix}. \tag{10}$$

In this case, there is no stress in the z direction, which means $\sigma_z = C_{13}\epsilon_x + C_{13}\epsilon_y + C_{33}\epsilon_z = 0$. Therefore, the strain in the z direction would be

$$\epsilon_z = -\frac{C_{13}}{C_{33}}(\epsilon_x + \epsilon_y).$$

The polarization in the z direction P_z is given by

$$P_z = P_{\rm sp} + \left(e_{13} - e_{33}\frac{C_{13}}{C_{33}}\right)(\epsilon_x + \epsilon_y) \tag{11}$$

where e_{ij} is the piezoelectric constant and $P_{\rm sp}$ is the spontaneous polarization of the piezoceramics, which is -0.26 C/m^2 for BaTiO$_3$. The dielectric constant ε_{33} of BaTiO$_3$ is $48\varepsilon_0$. The piezoelectric constants and elastic constants of BaTiO$_3$ are listed on Table II.

B. Thermal Sensor

We now consider how a fixed polar charge (and consequently the 2DEG) are influenced by the temperature changes. Polar oxides are not only good piezoelectric materials but also have good pyroelectric properties especially near Curie temperature. Pyroelectricity results from the temperature dependence of spontaneous polarization P_s of polar materials whether they are single domain single crystals or poled ceramics. Therefore, the pyroelectric coefficient is given by

$$p_g(T) = p + E\frac{\partial \varepsilon}{\partial T} \tag{12}$$

where p is the real pyroelectric coefficient and p_g is called generalized pyroelectric coefficient. As the temperature changes from T_0 to T, the spontaneous polarization of the oxide can be expressed by

$$P_{\rm sp}(T) = P_{\rm sp}(T_0) + p\Delta T. \tag{13}$$

Therefore, for thermal sensors, one needs to consider the changes in the spontaneous polarization when the temperature changes. Equation (11) will be modified to $P_z = P_{\rm sp}(T)$. Once the polarization P_z is obtained, the 2DEG induced by the polarization can be calculated by a charge-control model,

which solves Poisson equation and Schrödinger equation self-consistently.

C. Charge Control Model

We will now describe the charge control model to examine how changes in fixed polar charge influence 2DEG. The charge control model used has been successfully applied to treat piezoelectric and spontaneous polarization for the AlGaN–GaN FETs by several groups [18], [19], [22]–[24]. It also has been applied to calculate the response of ferroelectric materials grown on silicon [10]. For the charge control model, the semiconductor interface is treated as an ideal interface with abrupt transition from the channel materials to the barrier materials. To consider the piezoelectric polarization and spontaneous polarization effect, we apply the boundary condition for the heterojunction interface in the first step

$$\varepsilon_1 \mathbf{E_1} + \mathbf{P_1} = \varepsilon_2 \mathbf{E_2} \tag{14}$$

where ε_1 and ε_2 are the dielectric constants and $\mathbf{E_1}$ and $\mathbf{E_2}$ are electric fields at the interface. $\mathbf{P_1}$ are the polarization and can be calculated by (11). It also needs to satisfy another boundary condition at the interface expressed by

$$E_{c1} + \Delta E_c = E_{c2} \tag{15}$$

where E_c is conduction band energy profile which can be expressed as $\nabla \mathbf{E}$. ΔE_c is conduction discontinuity at the abrupt heterojunction interface. Once the boundary condition is decided, we can write down the Poisson equation

$$\nabla^2 E_c = -\frac{\rho}{\varepsilon} \tag{16}$$

where ρ is the total charge density and ε is the dielectric constant. The variation of fixed polar charges, dielectric constant, free electron charges distribution, and doping is along the z direction. Therefore we use the one dimensional Poisson equation

$$\frac{d^2}{dz^2} E_c(z) = -\frac{\rho(z)}{\varepsilon(z)}. \tag{17}$$

The total charge $\rho(z)$ is

$$\rho(z) = q\left(N_d^*(z) - N_a^*(z) - n_{\text{free}}(z) + p_{\text{free}}(z) - \sum_i n_i \psi_i^*(z)\psi_i(z)\right) \tag{18}$$

where N_d^* and N_a^* are the effective doping concentrations, which can be expressed as

$$N_d^* = N_d \frac{1}{1 + 2e^{\frac{(E_f - E_d)}{k_B T}}} \tag{19}$$

$$N_a^* = N_a \frac{1}{1 + 4e^{\frac{(E_a - E_f)}{k_B T}}} \tag{20}$$

where N_d and N_a are the concentration of donor and acceptor dopants and E_d and E_a are the impurity ionization energies. $n_{\text{free}}(z)$ and $p_{\text{free}}(z)$ are the free carrier concentrations in the bulk region, which can be expressed as

$$n_{\text{free}}(z) = N_c F_{\frac{1}{2}}\left(\frac{E_f - E_c(z)}{k_B T}\right) \tag{21}$$

$$p_{\text{free}}(z) = N_v F_{\frac{1}{2}}\left(\frac{E_v(z) - E_f}{k_B T}\right) \tag{22}$$

where N_c and N_v are the material effective density of states and $F_{1/2}$ is a half-order Fermi integral. $E_v(z)$ is the valence band energy and the sum over i in (18) is over 2-D confined subbands with normalized envelope functions, ψ_i, and occupation, n_i (p_i for the hole case). In the electron case, we can write the occupation

$$n_i = \frac{m_i k_B T}{\pi \hbar^2} \ln\left[1 + \exp\left(\frac{E_i - E_f}{k_B T}\right)\right] \tag{23}$$

where m_i is the in-plane effective mass and E_i is the subband level. In order to determine the 2-D confined subband envelope functions, ψ_i, and subband levels, E_i, we must solve the Schrödinger equation. The one dimensional Schrödinger equation can be written using the perpendicular part of the effective mass tensor as follows:

$$\frac{d^2}{dz^2}\psi_i(z) + \frac{2m_e}{\hbar^2}\left[E_i - E_c(z)\right]\psi_i(z) = 0 \tag{24}$$

where m_e is the effective mass along the quantum confinement direction. Once the Schrödinger equation has been solved, it is straightforward to obtain charge density using (23). The n_i and ψ_i obtained from (23) and (24) are fed into Poisson equation again and the equations are solved self-consistently.

III. Results

We will now present some typical results for the sensor-transitor. As noted in the introduction section, there is little on polar properties of when the film thickness approached ~ 20 Å. We will use the values reported in the literature for thick films. We will then also show, for comparison, how the results change if the polar parameters change dramatically at small thickness.

To study the performance of the sensor-FETs, we first begin with Si–SiO_2–$BaTiO_3$ heterostructure junctions. The layer thickness of SiO_2 is fixed at 8 Å in the simulation. Table I lists the parameters used in the calculation. Traditionally, silicon is used for mechanical sensors, because it combines well-established electronic properties with excellent mechanical properties [25]. Additionally, it would be very easy to integrate with other electronic circuits and microprocessors. Therefore, the material of the cantilever is assumed to be silicon in this case. The Young's modulus and Poisson ratio for silicon are 130 Gpa and 0.28, respectively [26]. The Schottky-barrier height is assumed 1.5 eV.

The purpose of the simulation is to shed light on two issues: 1) What is the variation of the 2DEG with strain? 2) What is the optimum thickness of the $BaTiO_3$ layer for a sensitive sensor-transistor? In Fig. 5, we show how the sheet charge density in the channel changes as stress increases. In Fig. 5(a), we show the 2DEG at the SiO_2–$BaTiO_3$ junction while in Fig. 5(b), it is

TABLE I
MATERIAL PARAMETERS USED IN THE CALCULATION—BANDGAP, ELECTRON EFFECTIVE MASS, HEAVY HOLE EFFECTIVE MASS, LIGHT HOLE EFFECTIVE MASS, DIELECTRIC CONSTANT, AND SPONTANEOUS POLARIZATION

Parameter	$BaTiO_3$	Si	SiO_2	AlN	GaN	GaAs	AlGaAs
E_g (eV)	3.1	1.12	9.0	6.2	3.4	1.424	1.79
m_e (m_0)	1.0	0.19	0.58	0.48	0.20	0.67	0.77
m_{hh} (m_0)	1.0	0.16	0.6	0.60	0.60	0.45	0.50
m_{lh} (m_0)	1.0	0.49	0.6	0.60	0.60	0.082	0.92
ε_{33} (ε_0)	48	11.9	3.9	9.14	10.4	13.18	12.244
P_{sp} (C/m^2)	-0.25	0	0	-0.081	-0.029	0	0

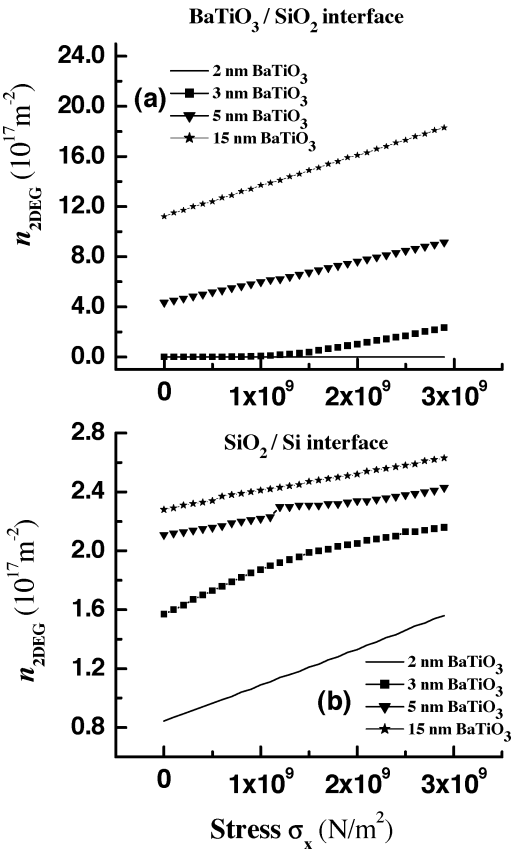

Fig. 5. Calculated sheet charge density, ($n_{2\mathrm{DEG}}$), at the Si–SiO_2–$BaTiO_3$ heterostructure junctions. (a) The $n_{2\mathrm{DEG}}$ at the SiO_2–$BaTiO_3$ interface; and (b) the $n_{2\mathrm{DEG}}$ at the Si–SiO_2 interfaces. The SiO_2 layer thickness is 8 Å. The gate voltage is 0 and the Schottky-barrier height is taken to be 1.5 eV.

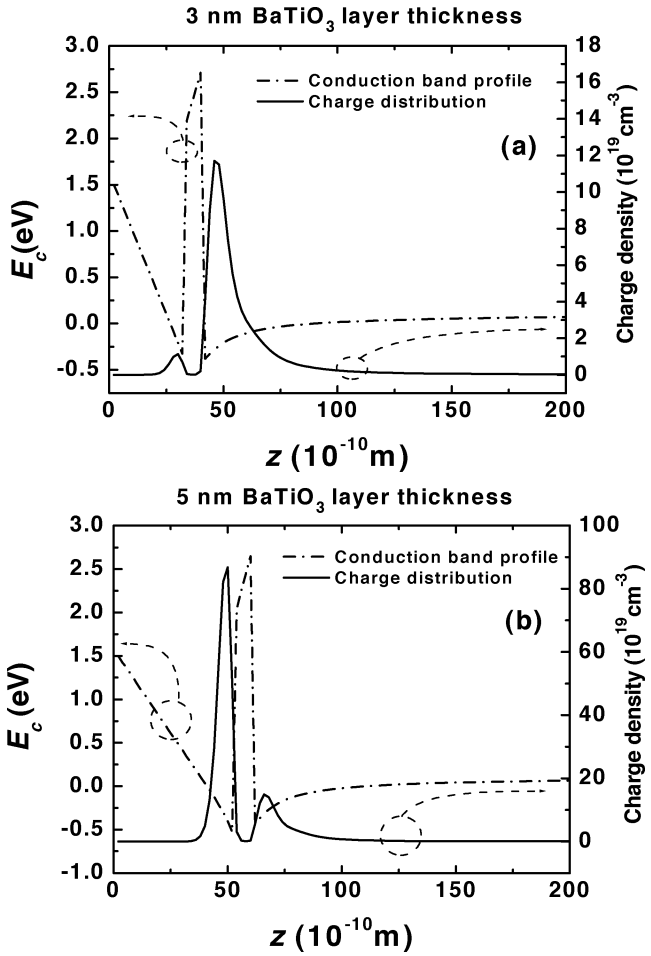

Fig. 6. Calculated charge density and conduction band profiles of Si–SiO_2–$BaTiO_3$ heterostructure junctions. (a) 30 Å $BaTiO_3$ layer thickness under stress $\sigma_x = 10^9$ N/m^2, and (b) 50 Å $BaTiO_3$ layer thickness under the same stress $\sigma_x = 10^9$ N/m^2. The SiO_2 layer thickness of is 8 Å. The gate voltage is 0 and Schottky-barrier height is taken to be 1.5 eV.

shown at the Si–SiO_2 junction. We see that for a 50 Å and 30 Å $BaTiO_3$ film, a large part of the electron free charge is at the SiO_2–$BaTiO_3$ interface. This is not desirable, as was discussed earlier. Fig. 6 shows the conduction band profile and charge density distribution for a 30 and a 50 Å $BaTiO_3$ layer thickness under a stress of 1×10^9 N/m^2. In Fig. 6(a), the charge density at the SiO_2–$BaTiO_3$ interface starts to increase, but for the 50 Å $BaTiO_3$ as seen in Fig. 6(b), it is clear most of the charge is accumulated at the SiO_2–$BaTiO_3$ interface. Since it is expected that mobile charge will have very poor transport properties and may cause deleterious trap related problems, it is important that the electron charge should reside at the Si–SiO_2 interface. We see that once $BaTiO_3$ thickness reaches 20 Å, the channel charge is all at the Si–SiO_2 interface and the device acts as a MOSFET but with a very large stress response.

To understand and compare the sensitivity of the stress sensor-FET and other stress sensors, we define the sensitivity of the cantilever to be

$$S = \frac{dn_{2\mathrm{DEG}}}{n_{2\mathrm{DEG}}} \frac{1}{dz} \tag{25}$$

$$= \frac{dn_{2\mathrm{DEG}}}{d\sigma_x} \frac{3Exd}{2L^3 n_{2\mathrm{DEG}}} \tag{26}$$

TABLE II
MATERIAL PARAMETERS FOR PIEZOELECTRIC MATERIALS—ELASTIC CONSTANT AND PIEZOELECTRIC CONSTANT

Parameter	$BaTiO_3$[21]	AlN	GaN [34]
C_{11} (Gpa)	211	410	370
C_{12} (Gpa)	107	140	145
C_{13} (Gpa)	114	100	110
C_{33} (Gpa)	160	390	390
e_{13} (C/m^2)	-3.88	-0.58	-0.34
e_{33} (C/m^2)	5.48	1.55	0.67
e_{15} (C/m^2)	32.6	-0.48	-0.30

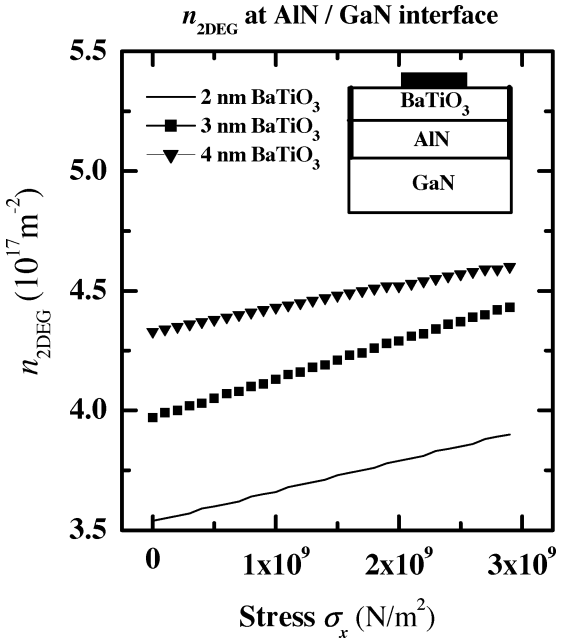

Fig. 7. Calculated sheet charge density, (n_{2DEG}), at the GaN–AlN heterostructure interface. The thickness of AlN layer is 30 Å. The gate voltage is 0 and Schottky-barrier height is taken to be 1.2 eV, respectively.

We find that the slope of $dn/d\sigma_x$ is equal to 2.57×10^7 N^{-1} for the optimal configuration. Therefore, we can obtain the sensitivity, S, is equal to 1.6×10^{-5} $Å^{-1}$. Compared to silicon piezoresistive cantilever [1], where the sensitivity, $\Delta R/Rz^{-1}$ is equal to 2.4×10^{-7} $Å^{-1}$, the sensor-FET has a superior potential performance. The change in channel charge shown in Fig. 5(b) will result in a change in the source-drain current if a standard FET is fabricated. As can be seen from Fig. 5(b), a large change in channel current is expected as stress changes.

We next consider GaN–AlN–$BaTiO_3$ heterojunctions. It is known there is a large spontaneous polarization in the nitrides. Additionally, the piezoelectric effect is also very strong, which is expected to induce large piezoelectric polarization under the strained conditions. Therefore, nitrides would be a good choice for piezoelectric sensors. The crystal structure of nitrides is wurtzite. The elastic constants, C_{ij} can also be expressed by (10), where C_{66} is $1/2[C_{11} - C_{12}]$. Therefore, the piezoelectric polarization induced by the strain would be the same as (11). It is noted that since the AlN is grown pseudomorphically on the GaN layer, there a static strain will be present in the

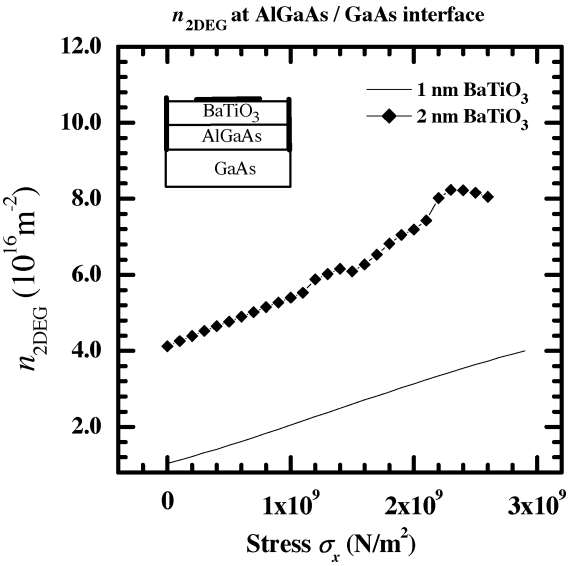

Fig. 8. Calculated sheet charge density, (n_{2DEG}), at the GaAs–$Al_{0.3}Ga_{0.7}As$ heterostructure interface. The thickness of $Al_{0.3}Ga_{0.7}As$ layer is 40 Å. The gate voltage is 0 and Schottky-barrier height is taken to be 1.5 eV.

AlN layer which would affect the polarization [17], [19]. The material of cantilever is assumed to be GaN in this calculation. The elastic constants and piezoelectric constants are listed in Table II. The Schottky-barrier height is assumed to be 1.2 eV in this case. From Table II we see that the piezoelectric constants of GaN and AlN are similar, which cancels part of the fixed polar charge variation at the GaN–AlN interface induced by the strain. Therefore, a structure with a thin $BaTiO_3$ layer on top is considered to improve the sensor properties. Fig. 7 shows a schematic of the structure and the results for using GaN–AlN–$BaTiO_3$ heterostructure junctions. Once again a large thickness of $BaTiO_3$ layer leads to higher band bending in $BaTiO_3$ layer and accumulation of sheet charge density at the AlN–$BaTiO_3$ interface. This would lower the performance of sensor and mobility of FETs channel. The optimal thickness of $BaTiO_3$ is 30 Å, for which the slope $dn/d\sigma_x$ is equal to 1.608×10^7 N^{-1}. The sensitivity of the cantilever is found to be 4.95×10^{-6} $Å^{-1}$.

For our final stress sensor case, we choose GaAs–$Al_{0.3}Ga_{0.7}As$–$BaTiO_3$ heterostructure junctions. The GaAs is assumed to be grown in (100) direction so that there is no piezoelectric effect. The Young's modulus and Poisson ratio are 85.5 GPa and 0.31 [27], respectively. The Schottky-barrier height is set to be 1.2 eV. Fig. 8 shows the sheet charge density versus stress σ_x for the GaAs–$Al_{0.3}Ga_{0.7}As$–$BaTiO_3$ heterostructure junctions. The slope, $dn/d\sigma_x$, is equal to 1.049×10^7 (N^{-1}). The sensitivity of GaAs cantilever is calculated to be 5.84×10^{-6} $Å^{-1}$. In this figure, we present the results for 10 and 20 Å $BaTiO_3$ layers. For large layer thickness cases $\geq$ 20 Å, the sheet charge density is mainly accumulated at the $Al_{0.3}Ga_{0.7}As$–$BaTiO_3$ interface, which is not suitable for the operation of sensor-FETs. Fig. 9 shows the conduction band profile and charge density distribution of 10 Å and 20 Å $BaTiO_3$ layer thickness. As shown in Fig. 9(b), The charge is mostly at the $Al_{0.3}Ga_{0.7}As$–$BaTiO_3$ interface. This is due to the smaller bandgap of $Al_{0.3}Ga_{0.7}As$ compared

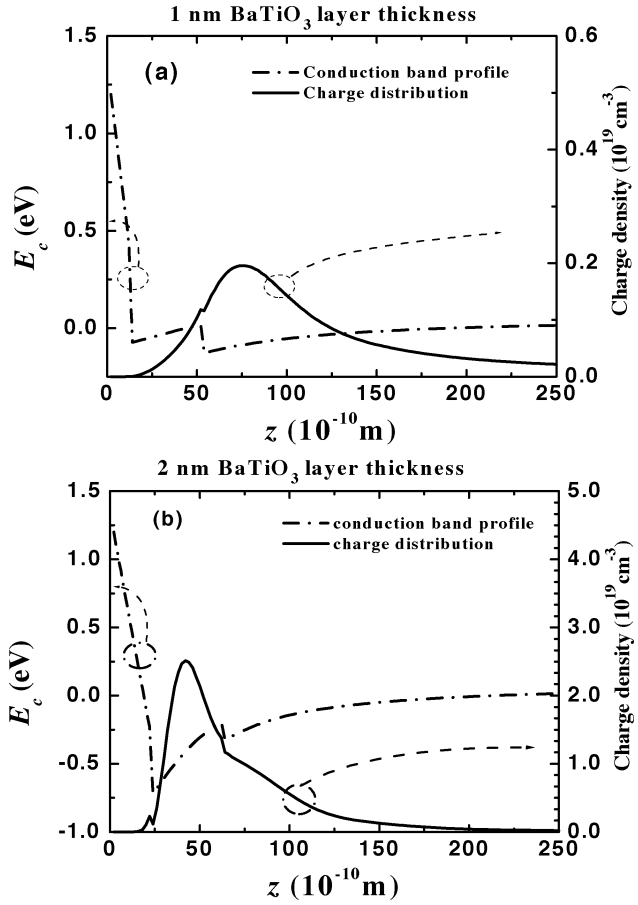

Fig. 9. Calculated charge density and conduction band energy profiles of GaAs–AlGaAs–$BaTiO_3$ heterostructure junctions. (a) 10 Å $BaTiO_3$ layer thickness under stress $\sigma_x = 10^9$ N/m^2; and (b) 20 Å $BaTiO_3$ layer thickness under stress $\sigma_x = 10^9$ N/m^2. The gate voltage is 0 and Schottky-barrier height is taken to be 1.2 eV.

to $BaTiO_3$. Therefore, the charge could not be confined well in the $Al_{0.3}Ga_{0.7}As$–GaAs interface, which limits the application of this device.

We will now discuss our results on the use of pyroelectric effect for the thermal sensor-FET. We choose the Si–SiO_2–$BaTiO_3$ heterostructure. The pyroelectric coefficient of $BaTiO_3$ at room temperature, T (300 K), has been reported to be -243 μC/m^{2}K [28]. This value compared to BST ($\sim$ 7000 μC/m^{2}K) or PST ($\sim$ 3500 μC/m^{2}K) [29], is relatively small. The pyroelectric coefficient changes as the temperature increases and dielectric constant also changes as the temperature increases. For temperature near the Curie temperature, ($T_c \sim 130$ °C), the pyroelectric coefficient has a peak and the spontaneous polarization becomes 0 at Curie temperature. In order to consider contributions of both pyroelectric coefficient and dielectric constant variation, we will directly fit the spontaneous polarization published in [30] as a function of temperature. The fitted pyroelectric coefficient for large scale temperature variation would be ~ -700 μC/m^{2}K.

As shown in Fig. 10, the changes in temperature would reduce the spontaneous polarization, which would decrease the sheet charge density at the Si–SiO_2 interface. It is found that the sheet charge density decreases from 8.45×10^{12} to 4.32×10^{12} (cm^{-2}), which shows that the device is very sensitive to

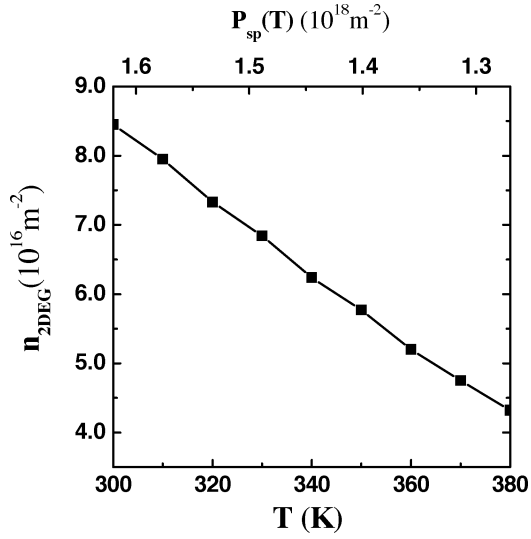

Fig. 10. Calculated sheet charge density, ($n_{2\mathrm{DEG}}$), versus temperature for the Si–SiO_2–$BaTiO_3$ heterostructure junctions. The thickness of $BaTiO_3$ layer is 20 Å and the thickness of SiO_2 layer is 8 Å.

changes in temperature. In order to compare the performance to other thermal sensors, the sensitivity of the thermal sensor-FET can be defined as

$$S = \frac{dn_{2\mathrm{DEG}}}{n_{2\mathrm{DEG}}}\frac{1}{dT} = \frac{dn_{2\mathrm{DEG}}}{dT}\frac{1}{n_{2\mathrm{DEG}}}. \tag{27}$$

By fitting the curve in Fig. 10, we can obtain $dn_{2\mathrm{DEG}}/dT = 5.24 \times 10^{14}$ (m^{-2}K^{-1}). Therefore, we can obtain the sensitivity S to be 6.2×10^{-3} (K^{-1}). A P-N diode thermal sensors typically have a variation in voltage of 2 mV/K. Thus the pyroelectric-FET should have better performance. To enhance the performance, larger pyroelectric coefficient materials such as BST and PST would be better choices. Otherwise, operating the FET thermal sensor near Curie temperature would be another choice. An issue that needs to be kept in mind is that pyroelectric materials with very high dielectric constants would reduce the band bending. Therefore, a larger layer thickness would be needed to obtain the same performance.

The parameters for oxides used in the calculations are assumed to be those for perfect bulk materials. However, in reality, the properties of thin-film piezoelectric or pyroelectric material may have differences from the bulk crystal. Recently, several theoretical and experimental reports [31], [32] indicate that the spontaneous polarization of $BaTiO_3$ would decrease when the film thickness is smaller than 100 Å. There are reports of a critical thickness, 24 Å for $BaTiO_3$ thin layer to keep its spontaneous polarization. The spontaneous polarization decrease to -0.05 C/m^2 at the critical thickness. Therefore, many experimentally obtained parameters of polar materials need to be determined. In order to determine the influences caused by parameter changes, we also examine the results for cases where the dielectric constant, ε_{33}, of $BaTiO_3$ varies from 48 [21] to 1900 [9] and spontaneous polarization P_{sp} varies from -0.26 C/m^2 to -0.05 C/m^2. Fig. 11 shows the calculated optimal $BaTiO_3$ layer thickness versus the dielectric constant for different spontaneous polarization. When the spontaneous

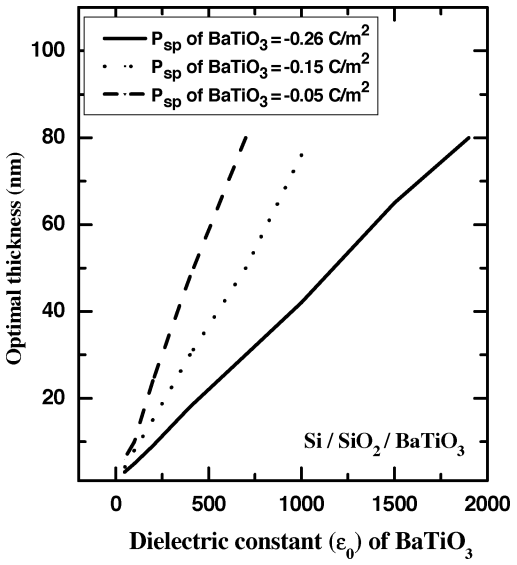

Fig. 11. Calculated optimal $BaTiO_3$ layer thickness of Si–SiO_2–$BaTiO_3$ heterostructure sensor-FETs for different dielectric constants and spontaneous polarization. The thickness of SiO_2 layer is 8 Å. The gate voltage is 0 and Schottky-barrier height is taken to be 1.5 eV. As discussed in the text, at the optimal thickness the 2DEG is located at the SiO_2–Si interface.

TABLE III
MATERIAL PARAMETERS FOR RELATED PIEZOELECTRIC MATERIALS

Parameter	$BaTiO_3$[21]	$LiNbO_3$[5]	$LiTaO_3$[5]	ZnO[35]
P_{sp} (C/m^2)	-0.26	-0.71	-0.50	-0.057
ε_{33} (ε_0)	48	28.6	43.7	9.9
ε_{11} (ε_0)	1600	82.9	52.6	
E_g (eV)	3.1	4.0	4.6	3.3
p (μC/m^{2}K)	238[28]		230[29]	
e_{13}(C/m^2)	-3.88	0.332	-0.143	-0.534
e_{33}(C/m^2)	5.48	1.896	1.804	1.200
e_{15}(C/m^2)	32.6	3.631	2.609	-0.48 [7]
e_{22}(C/m^2)		2.394	1.818	

polarization decrease to -0.05 C/m^2, the optimum $BaTiO_3$ changes from 30 Å to 60 Å. It is also clear that optimal polar material layer thickness is roughly proportional to $1/\varepsilon$. We can see that when ε is assumed to be be 1900 ε_0, we obtain an optimum layer thickness of ~ 800 Å. Thus if ε increases or spontaneous polarization decreases, the optimum thickness of polar materials increases. The parameter study of Fig. 11 would be useful for device design.

Table III lists the parameters of other polar materials that have potential to be used for sensor-FET applications. One must note that the use of polar oxides can also influence tunneling related to the gate current [33]. Another point to be kept in mind is that as a stress sensor, the sensitivity to temperature variation is undesirable. Therefore, choosing a high piezoelectric material with low pyroelectric coefficient would be suggested. Also as for most thermal sensor technologies, one more reference calibration sensor can be designed to cancel the variation caused by thermal variation.

IV. CONCLUSION

In this paper, we have examined how a material such as $BaTiO_3$ (with high piezoelectric response) can be combined with semiconductors to create a sensor-FET has a high sensitivity to stress. We have also examined how a pyroelectric material can be used in thermal sensors. Our results show that a very thin piezoelectric layer can allow a highly sensitive stress or thermal sensor as well as a high transconductance FET. This would allow sensor-FETs to be very small so that they can be very easily integrated into electronic circuits and microprocessors. The other advantage is that the sensor itself is already a power amplifier. The variation of free electron charge in the transistor channel is directly transconduced into the drain/source current which can be easily measured by current meter. Therefore, we can reduce the size of the sensor chip.

An important outcome of our study is that the thickness of the $BaTiO_3$ film is quite small (i.e., in the range of 10–30 Å). As a result, epitaxial growth technologies such as MBE are needed. However, this suggested thickness would change depending on the quality of thin ferroelectric film grown on the FET. The parameters used in our calculation are based on published results which are usually measured for thick films. For thin films, the polarization and dielectric constants may vary due to the quality the thin films. Our results provide motivations for experimental studies of heterostructure based on polar oxides and semiconductors.

In future work, we will examine the transport properties in the channel as well as trap affects at the interface.

REFERENCES

[1] J. Thaysen, A. Boisen, O. Hansen, and S. Bouwstra, "Atomic force microscopy probe with piezoresistive read-out and a highly symmetrical wheatstone bridge arrangement," *Sens. Actuators A, Phys.*, vol. 83, pp. 47–53, 2000.

[2] R. G. Beck, M. A. Eriksson, M. A. Topinka, and R. M. Westervelt, "GaAs–AlGaAs self-sensing cantilevers for low temperature scanning probe microscopy," *Appl. Phys. Lett.*, vol. 73, no. 8, pp. 1149–1151, 1998.

[3] A. K. Fung, L. Cong, J. D. Albrecht, M. I. Nathan, and P. P. Ruden, "Linear in-plane uniaxial stress effects on the device characteristics of AlGaAs–GaAs modulation doped field effect transistors," *J. Appl. Phys.*, vol. 81, pp. 502–505, 1997.

[4] M. Kimura and K. Toshima, "Thermistor-like pn junction temperature-sensor with variable sensitivity and its combination with a micro-air-bridge heater," *Sens. Actuators A, Phys.*, vol. 108, pp. 239–243, 2003.

[5] J. Kushibiki, I. Takanaga, S. Komatsuzaki, and T. Ujiie, "Chemical composition dependences of the acoustical physical contants of $LiNbO_3$ single crystal," *J. Appl. Phys.*, vol. 91, no. 10, pp. 6341–6349, May 2002.

[6] H. Ogi, Y. Kawasaki, and M. Hirao, "Acoustic spectroscopy of lithium niobate: elastic and piezoelectric coefficients," *J. Appl. Phys.*, vol. 92, no. 5, pp. 2451–2456, Sept. 2002.

[7] J. Gualtieri, J. Kosinski, and A. Ballato, "Piezoelectric materials for acoustic wave applications," *IEEE Trans. Ultrason., Ferroelect. Freq. Contr.*, vol. 41, no. 1, pp. 53–59, Jan. 1994.

[8] V. Gopalan and M. C. Gupta, "Observation of internal field in $LiTaO_3$ single crystals: its origin and time-temperature dependence," *Appl. Phys. Lett.*, vol. 68, no. 7, pp. 888–890, Feb. 1996.

[9] A. J. Moulson and J. M. Herbert, *Electroceramics*, 2nd ed. New York: Wiley, 2003, ch. 6, pp. 381–402.

[10] Y.-Y. Lin and J. Singh, "Study of ferroelectric-thin-film thickness effects on metal-ferroelectric-SiO_2-Si transistors," *J. Appl. Phys.*, vol. 91, no. 11, pp. 9297–9302, Jun. 2002.

[11] B. T. Liu, K. Maki, Y. So, V. Nagarajan, R. Ramesh, J. Lettieri, J. H. Haeni, D. G. Schlom, W. Tian, X. Q. Pan, F. J. Walker, and R. A. McKee, "Epitaxial La-doped $SrTiO_3$ on silicon: a conductive template for epitaxial ferroelectrics on silicon," *Appl. Phys. Lett.*, vol. 80, no. 25, pp. 4801–4803, Jun. 2002.

[12] B. Shen, W.-P. Li, T. Someya, Z. xia Bi, J. Liu, H.-M. Zhou, R. Zhang, F. Yan, Y. Shi, Z.-G. Liu, Y.-D. Zheng, and Y. Arakawa, "Influence of ferroelectric polarization on the properties of two-dimensional electron gas in $Pb(Zr_{0.53}Ti_{0.47})O_3$–$Al_xGa_{1-x}N$–GaN structures," *Jpn. J. Appl. Phys.*, pt. 1, vol. 41, no. 4B, pp. 2528–2530, Apr. 2002.

[13] A. Schmehl, F. Lichtenberg, H. Bielefeldt, J. Mannhart, and D. G. Schlom, "Transport properties of $LaTiO_{3+x}$ films and heterostructures," *Appl. Phys. Lett.*, vol. 82, no. 18, pp. 3077–3079, May 2003.

[14] A. P. Dmitriev, V. Y. Kachorovskii, M. S. Shur, and R. Gaska, "Nonlinear screening of pyroelectric films and grains in semiconductor matrix," *J. Appl. Phys.*, vol. 94, no. 1, pp. 566–572, Jul. 2003.

[15] O. J. Aldraihem and A. A. Khdeir, "Smart beams with extension and thickness-shear piezoelectric actuators," *Smart. Mater. Struct.*, vol. 9, pp. 1–9, 2000.

[16] F. Bernardini, V. Fiorentini, and D. Vanderbilt, "Spontaneous polarization and piezoelectric constant of III-V nitrides," *Phys. Rev. B, Condens. Matter*, vol. 56, no. 16, pp. 10 024–10 027, Oct. 1997.

[17] O. Ambacher, J. Smart, J. R. Shealy, N. G. Weimann, K. Chu, M. Murohy, W. J. Schaff, L. F. Eastman, R. Dimitrov, L. Wittmer, M. Stutzmann, W. Rieger, and J. Hilsenbeck, "Two-dimensional electron gases induced by spontaneous and piezoelectric polarization charges in N- and Ga-face AlGaN–GaN heterostructures," *J. Appl. Phys.*, vol. 85, no. 6, pp. 3222–3233, Mar. 1999.

[18] Y. Zhang and J. Singh, "Charge control and mobility studies for an AlGaN–GaN high electron mobility transistor," *J. Appl. Phys.*, vol. 85, no. 1, pp. 587–594, Jan. 1999.

[19] Y. Zhang, I. P. Smorchkova, C. R. Elsass, S. Keller, J. P. Ibbetson, S. Denbaars, U. K. Mishra, and J. Singh, "Charge control and mobility in AlGaN–GaN transistors: experimental and theoretical studies," *J. Appl. Phys.*, vol. 87, no. 11, pp. 7981–7987, Jun. 2000.

[20] M. Singh, Y. Zhang, J. Singh, and U. Mishra, "Examination of tunnel junctions in the AlGaN–GaN system: consequences of polarization charge," *Appl. Phys. Lett.*, vol. 77, no. 12, pp. 1867–1869, Sept. 2000.

[21] Z. Li, S.-K. Chan, M. H. Grimsditch, and E. S. Zouboulis, "The elastic and electromechanical properties of tetragonal $BaTiO_3$ single crystals," *J. Appl. Phys.*, vol. 70, no. 12, pp. 7327–7332, Dec. 1991.

[22] B. Jogai, "Free electron distribution in AlGaN–GaN heterojunction field-effect transistors," *J. Appl. Phys.*, vol. 91, no. 6, pp. 3721–3729, Mar. 2002.

[23] N. Maeda, T. Saitoh, K. Tsubaki, T. Nishida, and N. Kobayashi, "Enhanced effect of polarization on electron transport properties in AlGaN–GaN double-heterostructure field-effect transistors," *Appl. Phys. Lett.*, vol. 76, no. 21, pp. 3118–3120, May 2000.

[24] S.-H. Park and S.-L. Chuang, "Spontaneous polarization effects in wurtzite GaN–AlGaN quantum wells and comparison with experiment," *Appl. Phys. Lett.*, vol. 76, no. 15, pp. 1981–1983, Apr. 2000.

[25] K. E. Peterson, "Silicon as a mechnical material," *Proc. IEEE*, vol. 70, pp. 420–457, 1992.

[26] E. Anastassakis and M. Siakavellas, "Elastic properties of textured diamond and silicon," *J. Appl. Phys.*, vol. 90, no. 1, pp. 144–152, Jul. 2001.

[27] S. M. Sze, *Semiconductor Sensors*. New York: Wiley, 1994, ch. Appendix D, p. 535.

[28] A. Govindan, A. Tripathi, T. Goel, and P. Pillai, "Pyroelectric and piezoelectric studies on $BaTiO_3$: silica glass composites," in *Proc. Int. Symposium **AUTHOR Pls provide name of symposium?*** , September 1991, pp. 524–529.

[29] A. J. Moulson and J. M. Herbert, *Electroceramics*, 2nd ed. U.K.: Wiley, 2003, ch. 7, p. 420.

[30] W. J. Merz, "Double hysteresis of $BaTiO_3$ at the Curie point," *Phys. Rev.*, vol. 91, no. 3, pp. 513–517, Aug. 1953.

[31] J. Junquera and P. Ghosez, "Critical thickness for ferroelectricity in perovskite ultrathin films," *Nature*, vol. 422, pp. 506–509, Apr. 2003.

[32] M. G. Stachiotti, "Ferroelectricity in $BaTiO_3$ nanoscopic structures," *Appl. Phys. Lett.*, vol. 84, no. 2, pp. 251–253, January 2004.

[33] Y.-R. Wu, M. Singh, and J. Singh, "Gate leakage suppression and contact engineering in nitride heterostructures," *J. Appl. Phys.*, vol. 94, no. 9, pp. 5826–5831, Nov. 2003.

[34] O. Ambacher, J. Majewski, A. Link, M. Hermann, M. Eickhoff, M. Stuzmann, F. Bernardini, V. Fiorentini, V. Tilak, B. Schaff, and L. F. Eastman, "Pyroelectric properties of Al(In)GaN–GaN hetero- and quantum well structures," *J. Phys., Condens. Matter*, vol. 14, pp. 3399–3434, 2002.

[35] Y. Noel, C. M. Zicovich-Wilson, B. Civalleri, P. D'Arco, and R. Dovesi, "Polarization properties of ZnO and BeO: An *ab initio* study through the berry phase and wannier functions approaches," *Phys. Rev. B, Condens. Matter*, vol. 65, pp. 014 111-1–014 111-9, Dec. 2001.

Yuh-Renn Wu (M'03) received the B.S. degree in physics, and the M.S. degree in communication engineering from National Taiwan University, Taipei, Taiwan, in 1998 and 2000, respectively. He is currently pursuing the Ph.D. degree in Electrical Engineering at the Department of Electrical Engineering and Computer Science, University of Michigan, Ann Arbor.

His current research includes theoretical studies of vertical and parallel transport in III-V nitride heterostructures, ferroelectrics and opto-electronic devices.

Jasprit Singh received the Ph.D. degree in solid-state physics from the University of Chicago, Chicago, IL, in 1980 where he researched disordered semiconductors.

He then spent three years at the University of Southern California, Los Angeles, two years at Wright Patterson AFB, Ohio and has been at the University of Michigan, Ann Arbor since 1985. His area of research is physics and design of semiconductor heterostructure devices. He has worked on electronic and optoelectronic devices based on traditional III-V materials, HgCdTe, SiGe and the nitrides. Recently he is working on exploiting ferroelectric materials within conventional semiconductor devices. He has written seven textbooks, including *Modern Physics for Engineers,* (New York: Wiley Interscience, 1999) and *Semiconductor Devices: Basic Principles*, (New York: Wiley, 2001).